

ADVANCED MATERIALS

Supporting Information

for *Adv. Mater.*, DOI: 10.1002/adma.201503423

Progress of Flexible Electronics in Neural Interfacing – A
Self-Adaptive Non-Invasive Neural Ribbon Electrode for
Small Nerves Recording

*Zhuolin Xiang, Shih-Cheng Yen, Swathi Sheshadri, Jiahui
Wang, Sanghoon Lee, Yu-Hang Liu, Lun-De Liao, Nitish V.
Thakor, and Chengkuo Lee**

Supporting Information

Title : Progress of flexible electronics in neural interfacing – A Self-Adaptive Noninvasive Neural Ribbon Electrode for Small Nerves Recording

*Author(s), and Corresponding Author(s)**

*Zhuolin Xiang , Shih-Cheng Yen , Swathi Sheshadri, Jiahui Wang, Sang-Hoon Lee , Yu-Hang Liu, Lun-De Liao, Nitish V. Thakor , and Chengkuo Lee**

Zhuolin Xiang, Jiahui Wang, Sang-Hoon Lee and Prof. Chengkuo Lee
Department of Electrical & Computer Engineering, National University of Singapore, 4 Engineering Drive 3, Singapore 117576
Singapore Institute for Neurotechnology (SiNAPSE), National University of Singapore, 28 Medical Drive, #05-COR, Singapore 117456
Center for Intelligent Sensors and MEMS, National University of Singapore, 4 Engineering Drive 3, Singapore 117576
Email : elelc@nus.edu.sg

Prof. Shih-Cheng Yen, Swathi Sheshadri
Department of Electrical & Computer Engineering, National University of Singapore, 4 Engineering Drive 3, Singapore 117576
Singapore Institute for Neurotechnology (SiNAPSE), National University of Singapore, 28 Medical Drive, #05-COR, Singapore 117456

Prof. Nitish V. Thakor
Singapore Institute for Neurotechnology (SiNAPSE), National University of Singapore, 28 Medical Drive, #05-COR, Singapore 117456
Department of Biomedical Engineering, School of Medicine, Johns Hopkins University Baltimore, MD 21205, USA

Keywords: Flexible electronics, Peripheral neural interface, Small nerve, 3D electrode

Fabrication

The fabrication procedure follows standard photolithographic and clean room procedures. The detailed process is shown in Figure S1. Firstly, a 1 μm thick aluminum (Al) layer was evaporated on to the silicon substrate by physical vapor deposition (Figure S1 (a)). It acted as a sacrificial layer to release the final device from the substrate. Then a 5 μm base layer of photosensitive polyimide (Durimide 7005, Fujifilm, Japan) was spun onto the Al coated substrate with a speed of 2000 rpm. After exposed under ultraviolet (UV) with a dosage of 120 mJ/cm^2 , the base layer was post baked and developed in HTRD2 and RER 600 (Fujifilm, Japan), which defined the bottom layer pattern of the neural ribbon (Figure S1 (b)). The base polyimide layer was cured at 300 $^{\circ}\text{C}$ in N_2 for 0.5 h. This baking process is designed to only partially evaporate the water in the polyimide layer. In this way, it would bring a chemically and physically stable surface for the further processing while still leaving some unterminated bonds to attach the top polyimide layer ^[1]. After that, a layer of AZ 9260 (AZ Electronic Materials, USA) was spun on the polyimide base layer. This AZ layer was exposed and the electrode traces were patterned. A layer of 20 nm chrome (Cr) was deposited to improve the adhesion of following conduction layer by sputtering. After a 200 nm thick gold layer deposited (Figure S1(c)), the conductive metal layer was patterned by lift-off process in acetone (Figure S1(d)). Another 5 μm thick top layer of polyimide was spun on to the processed metal layer and patterned to expose sensing contacts and connection pad (Figure S1(e)). The inset of Figure S1 (e) demonstrated the concave openings of contacts. Then a 20 μm thick SU-8 2025 was spun on the polyimide layer. After development, the SU-8 protruding bumps were patterned exactly on the top of the sensing contacts (Figure S1 (g)). A stainless steel shadow mask was applied on the surface of the patterned neural ribbon device. Since the diameter of holes on the shadow mask was larger than the diameter of SU-8 bumps, the whole SU-8 protruding parts were fully exposed with a careful alignment. Then chip covered with the shadow mask was loaded on a rotational and inclined stage in the sputtering chamber. The whole SU-8 bumps as well as the underlying sensing contacts were sputtered with a layer of

300 nm Au (Figure S1 (h)). In this way, the whole SU-8 protruding bumps were enabled to be conductive structures.

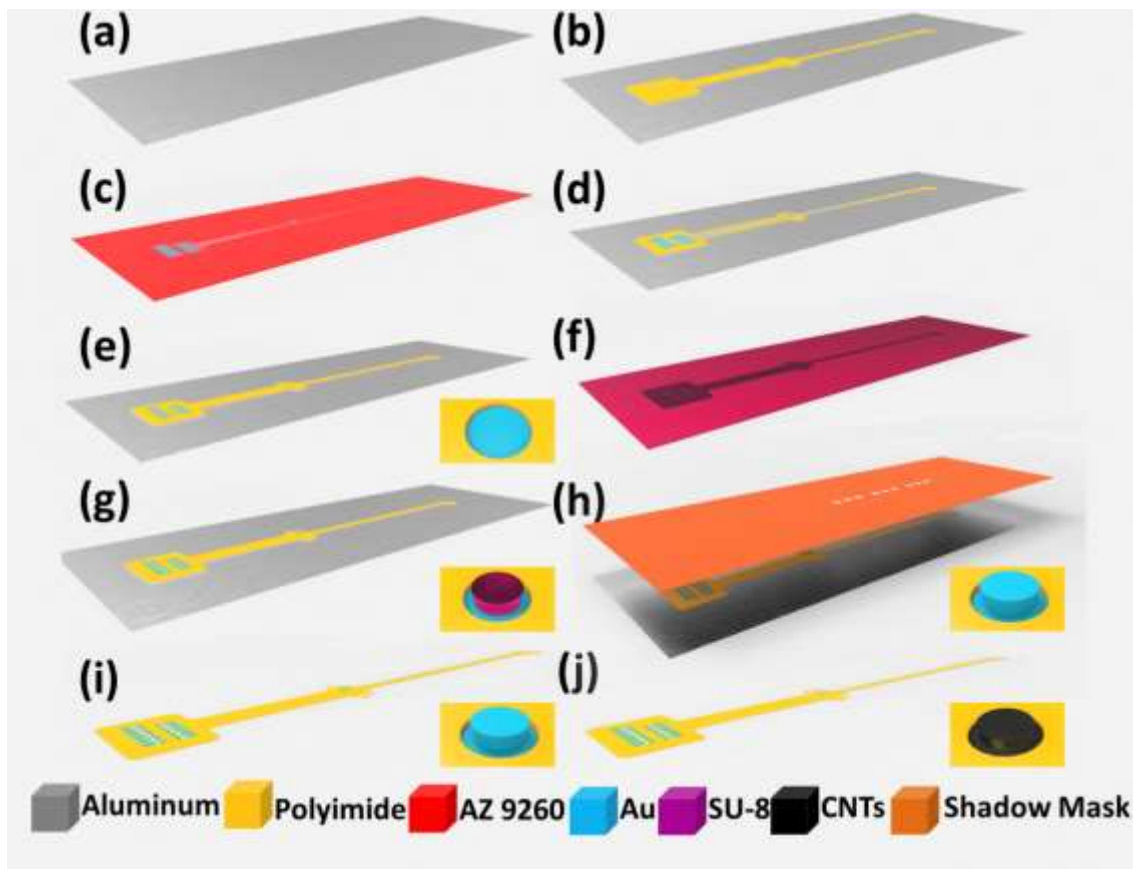


Figure S1. Fabrication process of the neural ribbon electrode.

The conventional approach to remove the sacrificial layer was wet etching process. However, the residue stress leads the released thin film structure to deform^[2]. Here, the anodic metal dissolution approach we adopted to release the whole device not only can ensure a flat released planar structure but also is significantly faster than the traditional wet etching process^[3]. The detailed releasing process is shown in our previous work^[4]. Briefly, the wafer was immersed in a 2 M NaCl solution and connected to an external positive terminal of a voltage source at 1V. A platinum (Pt) mesh electrode was connected to the negative terminal. A magnetic stir bar was also put inside the solution to keep a uniform NaCl concentration. After around 20 minutes, the exposed portions of the Al sacrificial layer were removed and only the covered portions of the Al sacrificial layer were left. Since the contact area between Al sacrificial

layer and NaCl solution decreases, the current dropped and Al etching rate reduced. Thus the voltage was then increased to 20 V to speed up the releasing process. After the whole Al sacrificial layer was removed in 2 hours, the final device could be released (Figure S1 (i)). Then the released device was packaged and a layer of carbon nanotubes were electroplated to minimize the impedance (Figure S1 (j)).

Device Packaging

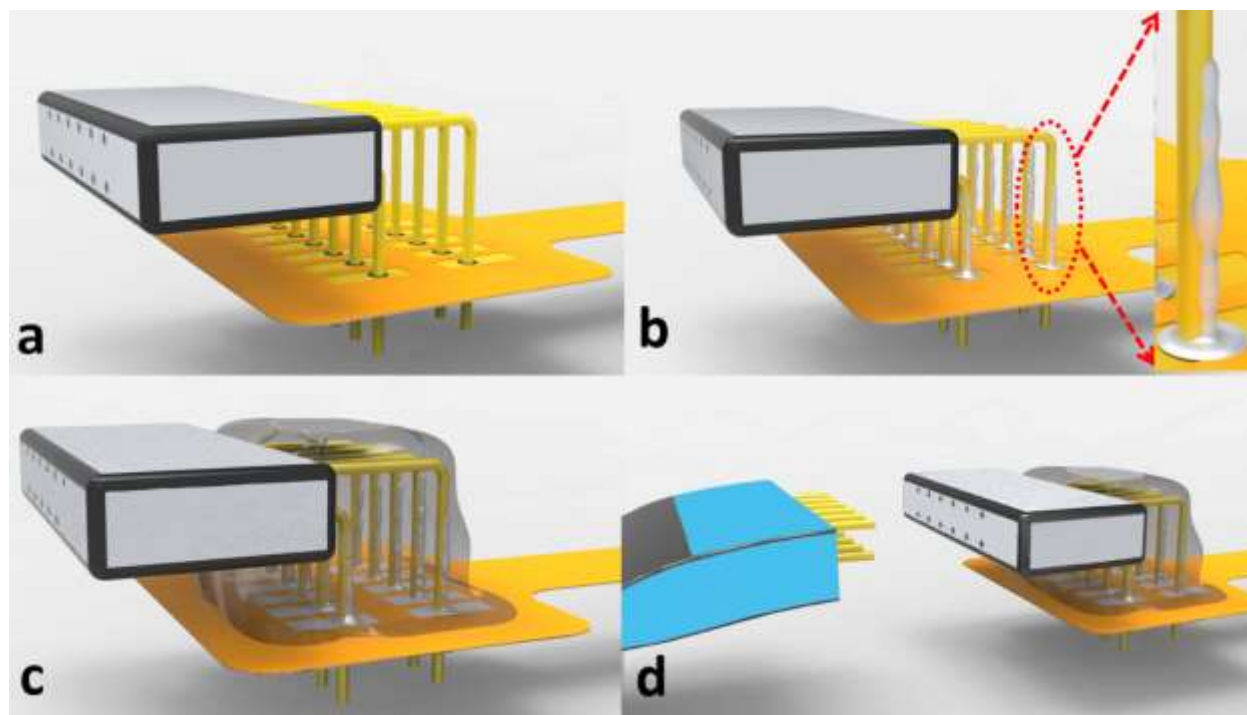


Figure S2 Illustration for the device packaging.

In order to perform the characterization of the neural ribbon device to obtain data from *in vitro* and *in vivo* tests, electrical interconnection needs to be conducted between the connection pads on the flexible substrate and terminals on the measurement equipment. However, it has been reported to be a challenging task if based on the conventional wire bonding technology ^[5]. Briefly, the soft polymer substrate may be damaged by the bonding tip and the electrodes pads on the flexible substrate are likely to delaminate during the bonding process ^[6]. In this study, in order to realize a reliable electrical interconnection, we used a customized Omnetics connector to package the final device. Figure S2 shows a schematic

overview of packaging approach. Since the geometry and dimension of the neural ribbon connection pads were specially designed to match with the customized connector as described before, the post contacts of the customized omnetics connector could be aligned with the underlying holes on the connection pad. By slightly pressing the backside of the neural ribbon substrate, these post contacts penetrated into holes and slotted to the end. A small drop of silver paste was then dipped on the top of the post contacts. The silver paste droplet was affected by gravitational force and flowed along the post contacts. It converged on the connection pad and was solidified after baked at 120 °C for half an hour. This method kept the silver paste from merging with the nearby pads, which was the common problem in the other packaging procedures. In order to ensure these connection joints were isolated from each other and the packaged device was biocompatible, a drop of medical UV adhesive (Henkel, USA) was applied to encapsulate the silver paste on the connection pads. Then the post contacts on the cable were plugged inside the holes on the customized omnetics connector. The other end of the cable was standard socket which matched with the measurement equipment ports.

Mechanical Testing

Since the neural ribbon is wrapped on the nerve bundle surface, the main concern to the wide acceptance of this device is the potential injury due to compressive pressure. The mechanical characteristic of the device was investigated. Tensile strength and elongation of five different prototypes were measured with Instron Microtester 5848 (Instron, USA). Strain was obtained with a velocity of 10 mm/min up to the break of the sample. The result is shown in Figure S3(a). When the strain was less than 7%, the polyimide neural ribbon was in a reversible linear range and the corresponding tensile strength was less than 0.74 N. When the strain was larger than 7%, the neural ribbon was in an irreversible deformed range and the device formed a neck in the central part. The tensile strength decreased above the 7% strain range and the device broke at higher elongation but at lower stress. With practice, we can tell the difference of neural ribbons at these two different states visually in the practical implantation process. Thus we can make sure

all the manipulation was carried out within the reversible range through visual observation during implantation process.

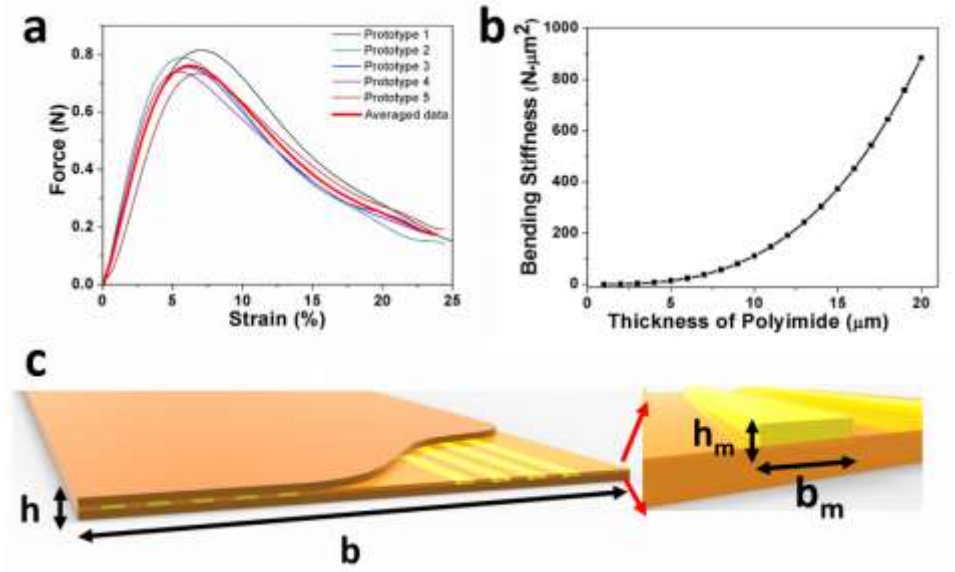


Figure S3 Mechanical characteristic of the neural ribbon electrode

Based on this measurement method, the device flexibility was investigated. According to the $\sigma = \frac{F}{A}$, the Young's Modulus of polyimide layer was calculated as 2.3G Pa. The cross sectional geometry of the sandwich device was shown in Figure S3(c). The bending stiffness of this structure could be obtained by the mathematic model given by Kim *et al* [7].

$$EI = E_{PI}bh\left(\frac{1}{3}h^2 - hy_0 + y_0^2\right) + (E_{Au} - E_{PI})nh_m b_m \left[\frac{1}{3}h_m^2 + h_m(h' - y_0) + (h' - y_0)^2\right]$$

Where E_{PI} and E_{Au} were Young's Modulus of polyimide layer and Au metal layer, size $b \times h$ and $b_m \times h_m$ were dimensions of polyimide layer and n gold bricks, y_0 was the distance between the neutral axis and bottom of the polyimide layer. Since the geometry of the neural ribbon was fixed by the designed mask and the thickness of metal layer was negligible compared with the whole device, the bending stiffness of the fabricated device was only depend on thickness of polyimide layer. We conducted the simulation to study their relationship. The result was shown in Figure S3 (b). The flexibility of the fabricated device

was excellent when the thickness was less than 10 μm . However, the rigidity of the device increased sharply when the thickness kept increasing. Considering that the neural ribbon need to have certain thickness for easier handling during the suturing in the practical experiment, 10 μm was chosen as the device thickness.

Impedance spectroscopy

The impedance of both Au recording contacts and CNT coated contacts were checked to compare the improved performance. Figure S4 (a) and Figure S4 (b) show the testing results. Impedance of both Au contacts and CNT coated contacts showed a considerable dependence on the frequency. Meanwhile, the impedance spectroscopy scan showed the CNT coated electrode contacts had the reduced impedance at all the measured frequencies. At the biologically relevant frequency of 1 kHz, the impedance of the Au electrode and the CNT coated electrode were 285.47 k Ω and 6.2 k Ω , respectively. It demonstrated that the 3D electrodes of the fabricated neural ribbon are significantly improved by CNTs electroplating. Tsang *et al.* attributed this enhancement to the nano-protrusions induced by the coated CNTs^[8]. The standard equivalent circuit model for the electrode-electrolyte interfacing is also shown in Figure S4 (a) and Figure S4 (b). A constant phase element ($Z_{dl} = 1/C_{dl}(j\omega)^n$, for an ideal capacitor $n=1$) presented the interface between the probe and saline. R_f was regarded as Faradaic impedance while R_s was taken as the spreading resistance of the solution. When the frequency increased from 10 Hz to 100 kHz, the constant phase element decreased as well as the total impedance. Compared with normal Au contacts, the charge injection capability increased on CNT coated contacts due to the induced nano-protrusions. Since the value C_{dl} was proportional to the charge injection capability, the total impedance of the CNT coated contacts at any certain frequency is smaller than that of the Au contacts. Thus, this CNT coating technique substantially improves the interfacial properties.

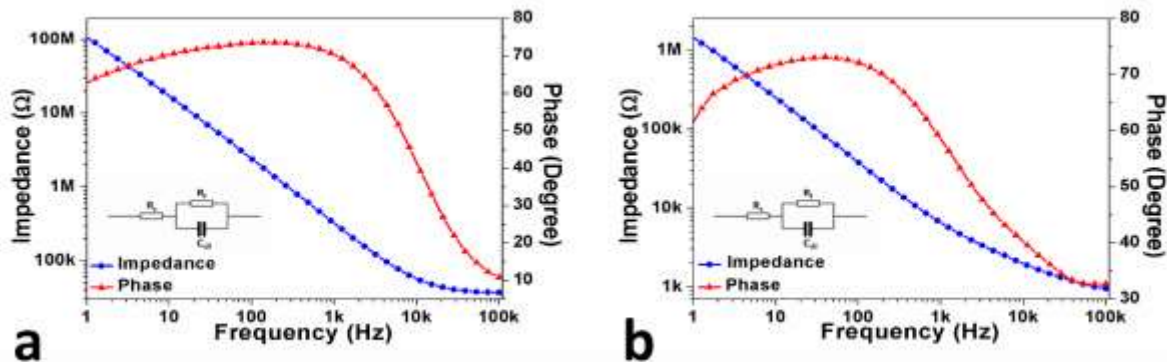


Figure S4 Impedance testing for the Au and CNT coated electrode.

Comparison of cuff electrode and neural ribbon electrode

The activated neural signals were recorded by both cuff electrode and neural ribbon electrode under the same stimulation. The results were used to compare the performance of the both electrodes. Figure S5 (a) and figure S5 (b) showed one representative recording from neural ribbon electrode and cuff electrode. The two signals exhibited parallel oscillations but with different quality. The recording from cuff electrode showed a higher noise level and more signal distortion compared with the signal from neural ribbon electrode. The statistical data acquired from 7 rats under the same testing condition were summarized to evaluate the performance of both electrodes. As shown in Figure S5 (c), the amplitude of neural signal from neural ribbon electrode is higher than the cuff electrode while its noise level is lower. The SNR of neural signal recorded by neural ribbon electrode is 3 times larger than the cuff electrode (SNR is based on absolute peak value/ 95th percentile noise value). The better signal quality is attributed to the improved contact between electrode and nerve body since the neural ribbon electrode is wrapped around the nerve body and there is minimum spacing between sensing site and epineurium.

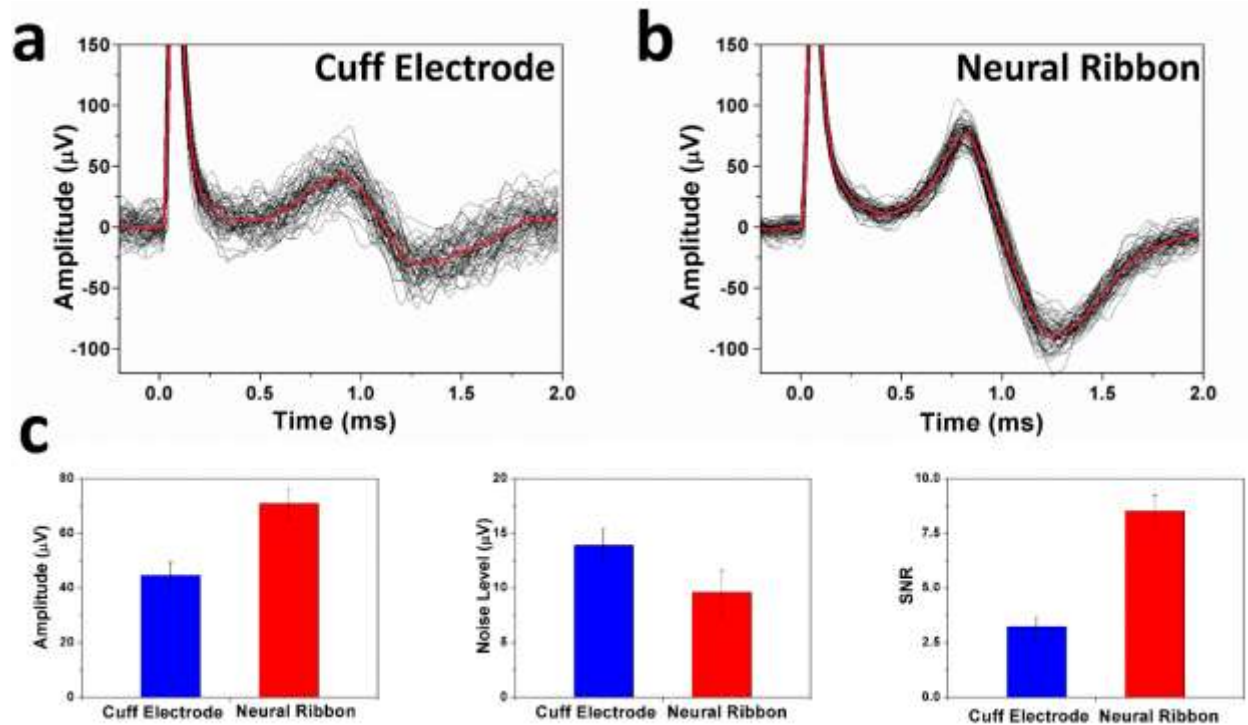


Figure S5 Figure 1 Compare between recordings from cuff electrode and neural ribbon electrode. The representative recordings from (a) cuff electrode and (b) neural ribbon electrode. The averaged data (red) is from 60 sets of recording data (black). (c) The signal amplitude, noise level and signal noise ratio (SNR) comparison between cuff electrode and neural ribbon electrode (values were based on mean \pm standard error, $n=7$)

- [1] D. F. Lemmerhirt, E. M. Staudacher, K. D. Wise, *IEEE Trans. Biomed. Eng.* **2006**, *53*, 2084.
- [2] W. Fang, J. A. Wickert, *J. Micromechanics Microengineering* **1996**, *6*, 301.
- [3] S. Metz, A. Bertsch, P. Renaud, *J. Microelectromechanical Syst.* **2005**, *14*, 383.
- [4] Z. Xiang, S.-C. Yen, N. Xue, T. Sun, W. M. Tsang, S. Zhang, L.-D. Liao, N. V Thakor, C. Lee, *J. Micromechanics Microengineering* **2014**, *24*, 065015.
- [5] C. Li, F. E. Sauser, R. G. Azizkhan, C. H. Ahn, I. Papautsky, *J. Micromechanics Microengineering* **2005**, *15*, 1729.
- [6] R. Ulrich, M. Wasef, J. Im, *PROCEEDINGS-SPIE* **1999**, *22*, 190.
- [7] D.-H. Kim, J. Viventi, J. J. Amsden, J. Xiao, L. Vigeland, Y.-S. Kim, J. A. Blanco, B. Panilaitis, E. S. Frechette, D. Contreras, *Nat. Mater.* **2010**, *9*, 511.
- [8] W. M. Tsang, A. L. Stone, D. Otten, Z. N. Aldworth, T. L. Daniel, J. G. Hildebrand, R. B. Levine, J. Voldman, *J. Neurosci. Methods* **2012**, *204*, 355.